The Journal of Chemical Physics

High resolution electronic spectroscopy of the $A\,^2\Sigma^- - X\,^2\Pi_{1/2}$ transition of PtN

Cite as: J. Chem. Phys. **141**, 084304 (2014); https://doi.org/10.1063/1.4893703
Submitted: 30 June 2014 . Accepted: 11 August 2014 . Published Online: 27 August 2014

Kaitlin Womack, Leah C. O'Brien, Sean Whittemore, James J. O'Brien, Anh Le, and Timothy C. Steimle

High resolution electronic spectroscopy of the $A\,^2\Sigma^- - X\,^2\Pi_{1/2}$ transition of PtN

Kaitlin Womack,[1] Leah C. O'Brien,[1,a)] Sean Whittemore,[2] James J. O'Brien,[2] Anh Le,[3] and Timothy C. Steimle[3]
[1]*Department of Chemistry, Southern Illinois University, Edwardsville, Illinois 62026-1652, USA*
[2]*Department of Chemistry and Biochemistry and Center for Nanoscience, University of Missouri, St. Louis, Missouri 63121-4400, USA*
[3]*Department of Chemistry, Arizona State University, Tempe, Arizona 96287-1604, USA*

(Received 30 June 2014; accepted 11 August 2014; published online 27 August 2014)

The (2,0) vibrational band of the $A\,^2\Sigma^- - X\,^2\Pi_{1/2}$ transition of platinum nitride, PtN, was recorded at Doppler-limited resolution using intracavity laser absorption spectroscopy (ILS) and at sub-Doppler resolution using molecular beam laser induced fluorescence (LIF) spectroscopy. Isotopologue structure for ^{194}PtN, ^{195}PtN, and ^{196}PtN, magnetic hyperfine splitting due to ^{195}Pt ($I = \frac{1}{2}$), and nuclear quadrupole splitting due to ^{14}N ($I = 1$) were observed in the spectrum. Molecular constants for the ground and excited states are derived. The hyperfine interactions are used to illuminate the nature of the $A\,^2\Sigma^-$ excited electronic state. © *2014 AIP Publishing LLC*. [http://dx.doi.org/10.1063/1.4893703]

INTRODUCTION

The platinum-ligand interaction plays a critical role in many areas of chemistry. For example, the platinum "*trans* effect," where in square planar Pt(II) chloride compounds ligands *trans* to the chloride are more easily replaced, is often exploited in inorganic synthesis. This phenomena is explained using qualitative arguments involving the σ and π interactions of the Pt-Cl bond.[1,2] Spectroscopic studies of small gas-phase Pt-containing molecules provide data on molecular and electronic structure and further insight into the nature of such interactions. Reactions of Pt-containing molecules provide a venue for experimentally probing these phenomena and other facets of catalysis in the absence of difficult-to-control, and poorly understood, chemical processes such as solvation, and aggregation.[3–5] While these simple model systems will never fully account for all the details of catalysis, they are amenable to theoretical calculations, and hence form a conceptual framework for understanding catalysis. Large scale applications where the Pt–N bond is relevant include NO_X reduction in car-exhaust catalytic treatments.[3] Here we describe the observation and analysis of a new spectral band of PtN that occurs near 852 nm. The band is assigned as the (2,0) $A\,^2\Sigma^- - X\,^2\Pi_{1/2}$ transition of PtN, where the fine and magnetic hyperfine structure determines the symmetry and the isotopic shifts of the transition energy determine the vibrational assignment.

A limited amount of experimental work has been reported for PtN. The optical spectrum was first identified in 1994 by Friedman-Hill and Field.[6] They observed and analyzed three distinct electronic transitions in the visible region between 16 500 and 18 600 cm^{-1}. Their work suggested that the ground state was of $^2\Pi_{1/2}$ symmetry. Using a laser ablation/molecular beam source, Jung *et al.*[7] recorded, both field-free and in the presence of a static electric field, the $|\Omega| = 1/2 - X^2\Pi_{1/2}$ band near 538 nm which had been identified by Friedman-Hill and Field.[6] Jung *et al.*'s work[7] included a high-level *ab initio* complete active space self-consistent field (CASSCF) treatment and first order configuration interaction (FOCI) computations on 10 low-lying electronic states of PtN from which the band was assigned as the (0,0) $d\,^4\Pi_{1/2} - X\,^2\Pi_{1/2}$ transition. Analysis of the ^{195}Pt ($I = 1/2$) magnetic hyperfine structure confirmed that the ground state was indeed of $X\,^2\Pi_{1/2}$ symmetry. The ^{14}N ($I = 1$) hyperfine splitting was not resolved in the work by Jung *et al.*,[7] but the electric dipole moments for the $d\,^4\Pi_{1/2}$ ($\upsilon = 0$) and $X\,^2\Pi_{1/2}$ ($\upsilon = 0$) states were determined to be 1.05(11) D and 1.977(9) D, respectively.

Calculations by Dai and Balasubramanian[8] extended the predictions of Ref. 7 to include 21 electronic states and applied more accurate multireference singles+doubles configuration interaction (MRSDCI) methods. Dai and Balasubramanian[8] also included relativistic spin-orbit effects and predicted the spectroscopic properties of the first six Ω-states. The spin-orbit splitting in the $X\,^2\Pi_r$ state was predicted[8] to be 2006 cm^{-1}, with a dominant (80%) $\cdots 3\sigma^2 1\pi^4 2\pi^1 1\delta^4$ electron configuration. Low-lying $^4\Sigma_{1/2}{}^-$ and $^2\Sigma_{1/2}{}^-$ states, with a dominant $\cdots 3\sigma^1 1\pi^4 2\pi^2 1\delta^4$ electron configuration, were predicted[8] at 889 cm^{-1} and 3449 cm^{-1}, respectively.

EXPERIMENTAL PROCEDURE

The PtN spectrum was recorded using two methods: mid-to-high *J*-lines were recorded at Doppler-limited resolution using intracavity laser spectroscopy (ILS); low *J*-lines were recorded using laser induced fluorescence (LIF) detection at sub-Doppler resolution in a supersonic molecular beam. The higher resolution, molecular beam spectra were used to

a)Author to whom correspondence should be addressed. Electronic mail: lobrien@siue.edu. Telephone: 618-650-3562.

characterize the ^{14}N hyperfine interaction and confirm the spectral assignment determined in the ILS work. For the ILS work, PtN molecules were produced in a plasma discharge sputter source with a 50 mm long Pt-lined hollow cathode; the method is similar to that used by us to produce PtF molecules.[9] The ILS approach used and further details on creating the plasma diatomic species is provided in Ref. 10. An applied potential produced a discharge current of 0.5 A in about 1.6 Torr of argon used as the sputter gas. Nitrogen gas was used as an oxidant and reacted with the platinum vapor generated from the cathode. PtN spectra from 11 620 through 11 738 cm^{-1} were recorded as a series of overlapping ~6 cm^{-1} wide spectral segments. The generation time[10] varied from 100 to130 μs which results in an effective pathlength of 0.92–1.2 km for a 50 mm long hollow cathode. Wavelength calibration was accomplished by alternatively measuring the spectrum of the intracavity PtN and the Doppler limited I_2 absorption spectrum recorded from an extra-cavity iodine cell heated to approximately 600 °C. The iodine atlas was used to calibrate the spectra.[11] Peak positions were determined from the zero crossing-points of the first derivative spectra using Savitzky–Golay polynomial smoothing, taking into account changes in the spectral dispersion across the multi-channel detector determined from ILS spectra of an intracavity etalon recorded in separate experiments.[12] The procedure enables the positions for isolated, unblended lines to be determined to an accuracy of better than ±0.007 cm^{-1}.

The molecular beam production and LIF detection schemes were similar to that used in the previous study.[7] A continuously rotating platinum rod was ablated in a supersonic expansion of approximately 5% ammonia (NH_3) seeded in argon with a backing pressure of approximately 3 MPa. The pulsed free-jet expansion was skimmed to form a well-collimated molecular beam which was crossed with a single longitudinal mode, continuous wave, Ti:Sapphire laser beam approximately 50 cm downstream from the source. The laser power was attenuated to approximately 50 mW and lightly focused (focal length = 1 m) to avoid power broadening. Spectral line widths of less than 40 MHz FWHM were observed. The absolute wavenumbers were determined to an accuracy of ±0.003 cm^{-1} by simultaneously recording the Doppler I_2 absorption spectrum.[11] Interpolation between I_2 absorption features was achieved by simultaneously recording the transmission of two confocal etalons. One etalon was actively stabilized and calibrated to have a free spectral range of 753 MHz. A second, unstabilized etalon with a free spectral range of 75 MHz was used to interpolate between transmission peaks of the stabilized etalon.

OBSERVATION

The ILS spectrum was recorded in the 11 620–11 738 cm^{-1} region. A portion of the ILS spectrum near 11 632 cm^{-1} is shown in Figure 1. Pronounced isotopologue structure is observed in the spectrum, and peaks due to the three most prominent isotopologues (^{194}PtN 33%, ^{195}PtN 34%, and ^{196}PtN 25%) were identified. For each rotational line, the separation between the outermost ^{194}PtN and ^{196}PtN

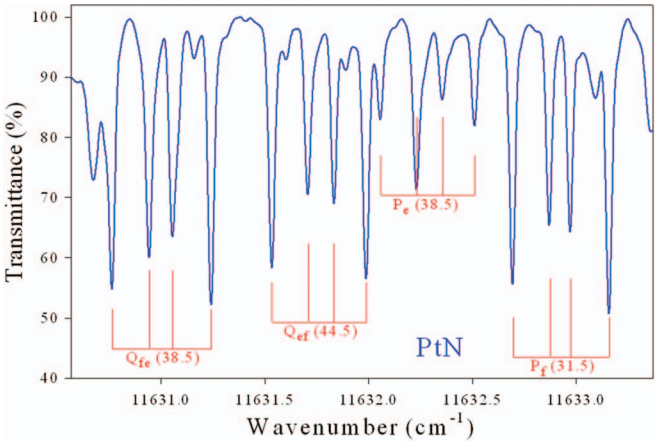

FIG. 1. Portion of ILS spectrum of PtN near 11 632 cm^{-1}.

peaks remained nearly constant throughout the spectrum at about 0.47 cm^{-1}, as displayed in Figure 1. The two smaller, middle peaks of each transition are the hyperfine components due to the nuclear spin of ^{195}Pt (I = 1/2), and this splitting is rather consistent at approximately 0.12 cm^{-1} at high J, although some small variation is observed in the different branches. Thus, a unique quartet pattern was observed throughout the spectrum. The band head at 11 738 cm^{-1} and the quartet pattern due to ^{194}PtN, ^{195}PtN, and ^{196}PtN are shown in Figure 2. Line positions, assignments, and residuals for all three isotopologues are presented in the supplementary material.[13]

The $R_1(1/2)$, $R_1(3/2)$, $R_{21}(1/2)$, $P_1(3/2)$, $Q_{21}(J = 1/2 - J = 9/2)$, and $Q_1(J = 1/2 - J = 5/2)$ branch features of the (2,0) $A\,^2\Sigma^- - X\,^2\Pi_{1/2}$ band for the ^{194}PtN isotopologue were recorded at high resolution using molecular beam LIF detection. Narrow LIF scans of $P_1(3/2)$ (ν = 11 728.728 cm^{-1}) and $Q_{21}(7/2)$ (ν = 11 731.204 cm^{-1}) branch features are given in Figure 3 along with the associated energy levels determined using the optimized molecular constants (*vide infra*). The small splitting of each branch feature is due to the ^{14}N (I = 1) hyperfine interaction. A comparison of various spectral features shows that the hyperfine interaction is substantial in both the $X^2\Pi_{1/2}$ (υ = 0) and the $A\,^2\Sigma^-$ (υ = 2) states. The

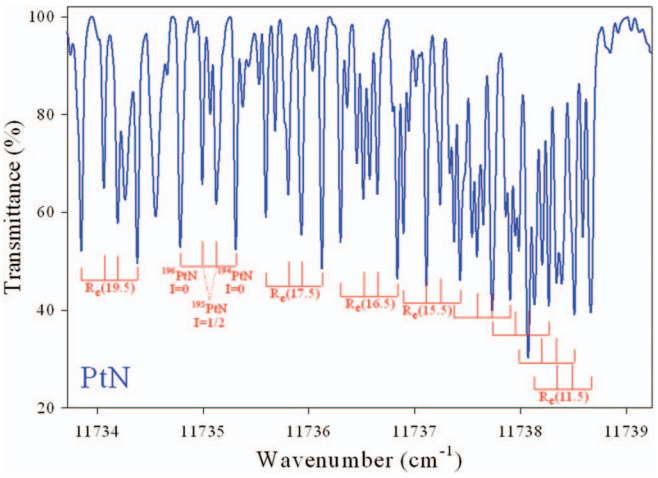

FIG. 2. ILS spectrum of PtN near bandhead at 11 738 cm^{-1}.

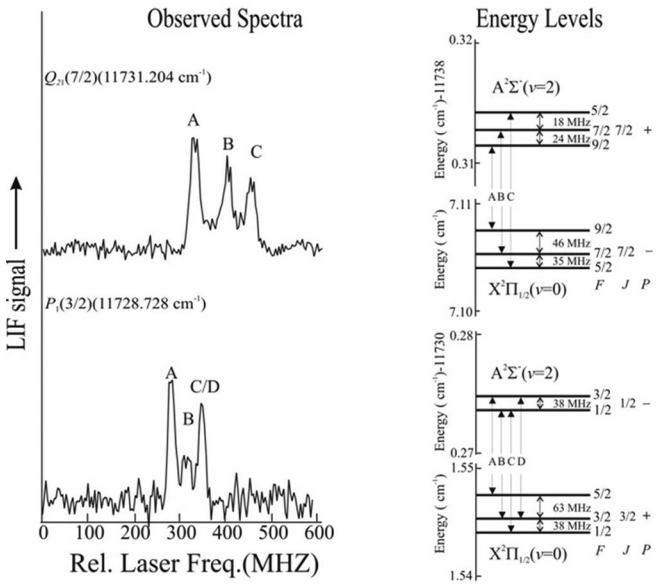

FIG. 3. Narrow LIF scans of $P_1(3/2)$ ($\upsilon = 11\,728.728$ cm^{-1}) and $Q_{21}(7/2)$ ($\upsilon = 11\,731.204$ cm^{-1}) branch features (left) along with the associated energy levels (right) obtained using the optimized parameters of Table II. The small splitting of each branch feature is due to the ^{14}N($I = 1$) hyperfine interaction.

assignments, observed ^{14}N ($I = 1$) hyperfine splitting of each line, and the differences from the calculated splitting for the 28 precisely measured splittings are presented in Table I.

ANALYSIS

Four strong branches were easily identified in the ILS spectrum. The lower state was assumed to be the ground $X\,^2\Pi_{1/2}$. Δ_2F and Δ_1F values for the ground state were predicted using the molecular constants from Jung *et al.*[7] and differences between the observed branches were tested in order to obtain rotational assignments. Ultimately the observed features were securely identified as the members of the R_{21}, Q_{21}, Q_1, and P_1 branches, confirming that the lower electronic state is $X\,^2\Pi_{1/2}$ ($\upsilon = 0$). Based on the initial fits of the ^{194}PtN lines, the weaker R_1 and P_{21} branches were predicted and subsequently identified for the ^{194}PtN and ^{196}PtN isotopologues.

There are two possibilities for the symmetry of the excited electronic state, either $^2\Sigma^+$ or $^2\Sigma^-$, and the data were fit both ways. The main difference in the excited state energy levels is the value of the spin-rotation parameter which we found to be $\gamma(^2\Sigma^+) = 1.628$ cm^{-1} or $\gamma(^2\Sigma^-) = 0.0398$ cm^{-1}. Previous calculations[7,8] predict a relatively low density of low-lying electronic states which suggest that the excited state γ value should be small, which supports the assignment of the observed spectrum as the $A\,^2\Sigma^- - X\,^2\Pi_{1/2}$ transition. The analysis of the ^{195}Pt ($I = 1/2$) magnetic hyperfine structure (*vide infra*) also supports the assignment of the excited state to be of $^2\Sigma^-$ symmetry.

Using vibrational frequencies calculated at the MRSDCI-level[8] for the $A^2\Sigma^-$ and $X\,^2\Pi_{1/2}$ states and the isotopologue relationships,[14] shifts for several possible excited state vibrational level assignments were predicted. The calculated origin shifts for the ^{194}PtN and ^{196}PtN isotopologues for the (0,0), (1,0), (2,0), and (3,0) bands of the $A\,^2\Sigma^- - X\,^2\Pi_{1/2}$ transition are −0.03, 0.21, 0.45, and 0.69 cm^{-1}, respectively. The observed origin shift of ∼0.47 cm^{-1} clearly supports the (2,0) vibrational band assignment for the transition.

Ultimately, the final fits of the Doppler limited ILS spectra were performed using PGOPHER 7.1.108,[15] with a separate fit for each isotopologue. The Hamiltonian utilized in the PGOPHER program can be separated into several standard components:[16]

$$\hat{H}_{rot} = B\hat{N}^2 - D\hat{N}^4 + H\hat{N}^6, \quad (1)$$

TABLE I. The assignments, observed ^{14}N hyperfine splitting, and the differences from the calculated splitting in (MHz) of the ^{194}PtN isotope in the (2,0) $A\,^2\Sigma^- - X\,^2\Pi_{1/2}$ band.

	A[a]		B[a]		Splitting A-B (MHz)			A[a]		B[a]		Splitting A-B (MHz)	
Line	F''	F'	F''	F'	Obs.	Diff.	Line	F''	F'	F''	F'	Obs.	Dif.
$Q_1(1/2)$	1.5	1.5	0.5	0.5	30	−2	$Q_{21}(3/2)$	1.5	1.5	2.5	2.5	94	0
	1.5	0.5	0.5	1.5	30	2		0.5	0.5	1.5	1.5	47	−9
$Q_1(3/2)$	2.5	2.5	1.5	1.5	52	6		2.5	1.5	2.5	2.5	64	1
$Q_1(5/2)$	3.5	3.5	2.5	2.5	45	−3	$Q_{21}(5/2)$	2.5	2.5	3.5	3.5	79	3
	2.5	2.5	1.5	1.5	39	5		1.5	1.5	2.5	2.5	56	1
	2.5	1.5	1.5	1.5	15	−1		3.5	2.5	3.5	3.5	48	−3
	3.5	2.5	2.5	2.5	22	1		2.5	1.5	2.5	2.5	32	−5
$P_1(3/2)$	0.5	1.5	1.5	2.5	41	8	$Q_{21}(7/2)$	3.5	3.5	4.5	4.5	73	3
	0.5	0.5	0.5	1.5	34	−5		2.5	2.5	3.5	3.5	54	0
	1.5	1.5	0.5	1.5	34	4	$Q_{21}(9/2)$	4.5	4.5	5.5	5.5	69	3
	1.5	0.5	2.5	1.5	98	−6		3.5	3.5	4.5	4.5	50	−4
	0.5	0.5	2.5	1.5	94	4	$R_{21}(1/2)$	1.5	1.5	2.5	1.5	30	1
$Q_{21}(1/2)$	0.5	1.5	1.5	1.5	48	−1	$R_1(3/2)$	2.5	1.5	3.5	2.5	43	2
	0.5	0.5	1.5	0.5	48	−1		1.5	0.5	2.5	1.5	22	0
												Std. dev. = 4 MHz	

[a]The "A" and "B" components are the higher and lower frequency spectral features, respectively, associated with a given measured splitting. For example, the first row under the $Q_{21}(7/2)$, entries are the quantum numbers for the "A" and "B" spectral features given in Figure 3 and the measured splitting between these two lines.

TABLE II. Molecular constants for the $A\,^2\Sigma^-$ ($\upsilon = 2$) and $X\,^2\Pi_{1/2}$ ($\upsilon = 0$) states of ^{194}PtN, ^{195}PtN, and ^{196}PtN (in cm^{-1} except where indicated). (One std. dev. in parenthesis).

		T_v	B	$D \times 10^7$	$p+2q$	$p_D \times 10^7$	$h_{1/2}(^{195}\text{Pt})$	$d(^{195}\text{Pt})$	$h_{1/2}(^{14}\text{N})$	$d(^{14}\text{N})$
$X\,^2\Pi_{1/2}\ \upsilon = 0$	^{194}PtN	0.0[a]	0.453 312(30)	4.05(14)	0.123 730(90)	6.91(73)			64(2) MHz	62(3) MHz
	^{195}PtN	0.0[a]	0.453 120 8[a]	3.63(11)	0.123 790(67)	5.43(65)	0.0639[a]	−0.0034[a]		
	^{196}PtN	0.0[a]	0.452 929(38)	3.33(19)	0.123 81(10)	4.42(84)				
	Lit.[b]		0.4541(7)		0.1219(15)					
		T_v	B	$D \times 10^7$	γ	$\gamma_D \times 10^6$	$b(^{195}\text{Pt})$	$c(^{195}\text{Pt})$	$b_F(^{14}\text{N})$	$c(^{14}\text{N})$
$A\,^2\Sigma^-\ \upsilon = 2$	^{194}PtN	11 731.117 14(69)	0.396 911(30)	4.79(13)	− 0.041 33(11)	5.570(98)			20(2) MHz	−58(6) MHz
	^{195}PtN	11 730.855 49(62)	0.396 736 3(19)	4.39(10)	− 0.041 509(93)	5.610[a]	0.2307(14)	0.0777(56)		
	^{196}PtN	11 730.587 21(77)	0.396 569(38)	4.12(18)	− 0.041 62(14)	5.65(11)				

[a]Value held constant in fit, see text.
[b]From Jung *et al.*[7]

$$\hat{H}_{spin\ orbit} = A\hat{L}_z\hat{S}_z \quad (^2\Pi \text{ only}), \tag{2}$$

$$\hat{H}_{spin\ rotation} = \gamma\hat{\boldsymbol{N}}\cdot\hat{\boldsymbol{S}} + \frac{1}{2}\gamma_D[\hat{\boldsymbol{N}}\cdot\hat{\boldsymbol{S}}, \hat{\boldsymbol{N}}^2]_+ \quad (^2\Sigma \text{ only}), \tag{3}$$

$$\begin{aligned}\hat{H}_{\lambda\ doubling} = &-\frac{1}{2}p(\hat{N}_+\hat{S}_+e^{-2i\phi} + \hat{N}_-\hat{S}_-e^{+2i\phi}) \\ &+\frac{1}{2}q(\hat{N}_+^2e^{-2i\phi} + \hat{N}_-^2e^{+2i\phi}) \\ &-\frac{1}{4}p_D[\hat{N}_+\hat{S}_+e^{-2i\phi} \\ &+\hat{N}_-\hat{S}_-e^{+2i\phi}, \hat{\boldsymbol{N}}^2]_+ \quad (^2\Pi \text{ only}),\end{aligned} \tag{4}$$

$$\begin{aligned}\hat{H}_{magnetic\ dipole} = &\ a\hat{\boldsymbol{I}}\cdot\hat{\boldsymbol{L}} + b_F\hat{\boldsymbol{I}}\cdot\hat{\boldsymbol{S}} + c/3(3\hat{I}_z\hat{S}_z - \hat{\boldsymbol{I}}\cdot\hat{\boldsymbol{S}}) \\ &-\frac{1}{2}d(\hat{S}_+\hat{I}_+e^{-2i\phi} + \hat{S}_-\hat{I}_-e^{+2i\phi}),\end{aligned} \tag{5}$$

$$\hat{H}_{electric\ quadrupole} = \frac{eQq_0}{4\hat{\boldsymbol{I}}(2\hat{\boldsymbol{I}}-1)}\left(3\hat{I}_z^2 - \hat{\boldsymbol{I}}^2\right). \tag{6}$$

The data is restricted to only the $|\Omega| = 1/2$ spin-orbit component of the $A^2\Pi$ state. Hence, only the linear combination of the Λ-doubling parameters, $p + 2q$, is determinable. Furthermore, only the effective magnetic hyperfine interactions parameter, $h_{1/2}$, and the parity dependent term, d, are determinable. The effective parameter h_Ω is related to the Frosch and Foley[17] parameters by $h_\Omega = a\Lambda + (b+c)\Sigma$,[18] where Λ and Σ are the molecular fixed axis projection of the total electronic orbital and spin angular momenta, respectively.

Fits of the ^{194}PtN and ^{196}PtN line positions were straightforward, and the molecular constants determined from the fits are presented in Table II. For the $X^2\Pi_{1/2}$ state, the B_0 values for these two isotopologues are consistent with the isotopologue relationships[14] within the experimental uncertainty. The molecular constants of the $X\,^2\Pi_{1/2}$ state from Jung *et al.*[7] are also included in Table II for comparison. In our work, as in the Jung *et al.*[7] analysis, the ground state $X\,^2\Pi$ term energy was set to 1000 cm^{-1} and the spin-orbit constant held fixed at +2000 cm^{-1}. This sets the term energy of $\upsilon = 0$ of the $X\,^2\Pi_{1/2}$ state at $T_0 = 0$ cm^{-1}.

The ^{195}PtN lines show well-resolved magnetic hyperfine structure in the ILS spectra due to the ^{195}Pt isotope ($I = 1/2$), with the majority of the features being assigned as $\Delta F = \Delta J$. Two distinct hyperfine patterns are evident in the spectrum: the R_{21} and Q_{21} lines gave similar splittings, and the P_1 and Q_1 lines gave similar splittings. This indicates that the magnetic hyperfine structure was mainly in the excited state. Initially, the analytical expressions of Townes and Schawlow[18] for the diagonal matrix elements of $\hat{H}_{hyperfine}$ in a Hund's case ($b_{\beta J}$) basis were used to model the hyperfine structure at high J values. Based on the splitting of the hyperfine components at high J, an estimate of $b(A\,^2\Sigma) = \pm 0.23$ cm^{-1} was obtained.

The LIF spectrum of the $R_{21}(0.5)$ line was used to confirm the symmetry of the excited $^2\Sigma$ state. As shown in Figure 4, the two main hyperfine components of the $R_{21}(0.5)$ line with $\Delta F = \Delta J$ were observed at 11 732.4367 and 11 732.5873 cm^{-1}, with the lower energy component weaker in intensity. Since the intensity is proportional to the degeneracy of the levels, the weaker transition is assigned as $F' = 1\text{e} \leftarrow F'' = 0\text{e}$, and the stronger transition is assigned as $F' = 2\text{e} \leftarrow F'' = 1\text{e}$. With this assignment, the sign of b_F was determined to be negative, which is not consistent with a $^2\Sigma^+$ state with a single, unpaired σ electron. Observation of two satellite lines, the $R_{21}(0.5)$ with $F' = 1\text{e} \leftarrow F'' = 1\text{e}$ at $\nu = 11\,732.389$ cm^{-1} and the $S_1(0.5)$ line with $F' = 2\text{f} \leftarrow F'' = 1\text{e}$ at $\nu = 11\,732.3095$ cm^{-1}, provides further support for

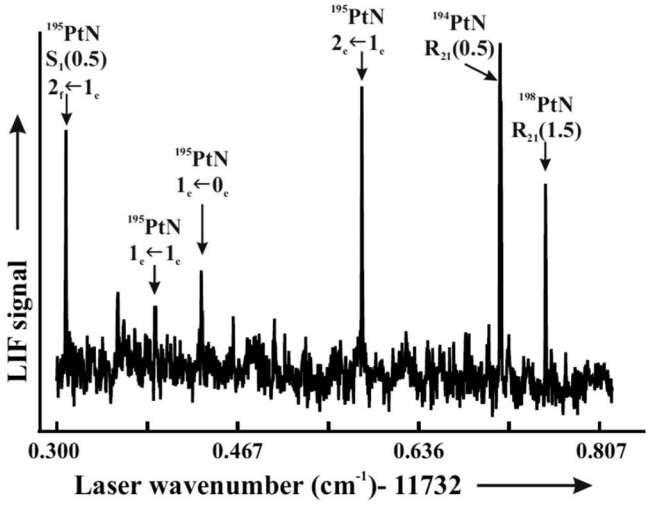

FIG. 4. Narrow LIF scan near the ^{195}PtN $R_{21}(0.5)$ branch feature. The total angular moment F' and F'' values are labelled for each peak associated with the ^{195}PtN hyperfine structure.

the rotational and hyperfine assignments and the excited state symmetry.

The ^{195}PtN isotopologue data set includes four regular branches with $\Delta F = \Delta J$, plus two $^{R}S_{1}(J)$ satellite lines with $\Delta F = +1$ at low J. The molecular constants from the initial fits exhibited high correlation and their uncertainties were significantly higher than those of the ^{194}PtN and ^{196}PtN parameters. To improve the fit, the ground state B_0 value for ^{195}PtN was fixed to that predicted from the ^{194}PtN B_0 value using the isotopologue relationships[14] and the excited state γ_D value was held fixed at the average of the γ_D values for ^{194}PtN and ^{196}PtN. In the final fit, the ground state hyperfine parameters were constrained to the previously determined values.[7] These conditions resulted in an acceptable fit for the line positions, with a standard deviation of <0.008 cm^{-1} for the ILS data and <0.004 cm^{-1} for the LIF data. The fitted molecular constants for ^{195}PtN are given in Table II.

The small ^{14}N splitting observed in the molecular beam LIF spectrum of ^{194}PtN was modelled using a separate program written specifically for this project. The eigenvalues and eigenvectors were obtained by diagonalization of matrix representations with dimensions of 12 (=2 × (2S + 1) × [2I(^{14}N) + 1]) for the $X\,^2\Pi_{1/2}$ ($v = 0$) state and 6 (=2 × (2S + 1) × [2I(^{14}N) + 1]) for the $A\,^2\Sigma^-$ ($v = 2$) state, constructed in the Hund's case ($a_{\beta J}$) basis set. The fine structure parameters were held fixed to the values determined from the analysis of the ^{194}PtN ILS data. The $X\,^2\Pi_{1/2}$ ($v = 0$) hyperfine energies were modelled with $h_{1/2}$ and d terms and those for the $A\,^2\Sigma^-$ ($v = 2$) state with the b and c terms. The small nuclear quadrupole interactions were not required. The 28 spectral splittings of Table I were used as input for a nonlinear least squares fitting procedure. The optimized parameters and associated errors are given in Table II. The standard deviation of the ^{14}N splitting was 4 MHz which is consistent with the measurement uncertainty.

DISCUSSION

The molecular orbital correlation diagram shown in Figure 5 was developed using a Fenske-Hall type calculation[19] to assist in the qualitative interpretations of the spectroscopic parameters. It is similar to the one used to explain the relative values of the electric dipole moment in the PtX (X = C, N, O, and S) series of molecules.[20] Analysis of the composition of the predicted molecular orbitals[7,8] shows that the 2π orbital is primarily a Pt($5d\pi$)-N($2p\pi$) anti-bonding orbital whereas the 3σ orbital is a mixture of the Pt($5d\sigma$), Pt($6s\sigma$), and N($2p\sigma$) orbitals. The relative contributions of these three atomic orbitals to the 3σ molecular orbital vary significantly with the electronic state.[7,8]

The molecular orbital correlation diagram indicates that the $X\,^2\Pi_r$ state arises from a dominant $\cdots 3\sigma^2 2\pi^1$ electronic configuration, which has been predicted through high-level *ab initio* calculations,[7,8] predicted from more recent density functional calculations,[21] and confirmed experimentally.[6,7] The molecular orbital correlation diagram indicates that the first excited electronic configuration is $\cdots 3\sigma^1 2\pi^2$, which gives rise to Hund's case (a) $^4\Sigma^-$, $^2\Sigma^-$, $^2\Delta$, and $^2\Sigma^+$ states. The low-lying $a\,^4\Sigma^-$ (T_e = 889 cm^{-1}) and $A\,^2\Sigma^-$ (T_e = 3449 cm^{-1}) states predicted from the high-level *ab initio* calculations[7,8] do indeed have a dominant $\cdots 3\sigma^1 2\pi^2$ configuration.

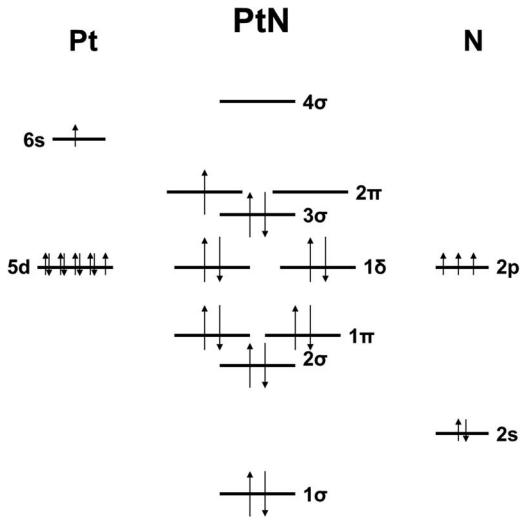

FIG. 5. Molecular orbital correlation diagram for the ground state of PtN.

Based upon the observed isotopic shifts, the present spectrum is assigned as the (2,0) $A\,^2\Sigma^- - X\,^2\Pi_{1/2}$ transition. The bond length in the $v = 2$ $A\,^2\Sigma^-$state, $r_2 = 1.803$ Å, is significantly longer than that for the $v = 0$ × $^2\Pi_{1/2}$ state where $r_0 = 1.687$ Å. The lengthening of the bond upon $3\sigma \rightarrow 2\pi$ excitation is consistent with a promotion of an electron from the non-bonding 3σ-orbital to the anti-bonding 2π orbital as implied by the molecular orbital correlation diagram, Figure 5.

Using the calculated vibrational frequency,[8] ω_e (=696 cm^{-1}), the experimental term energy, T_e, for the $A\,^2\Sigma^-$ state is estimated to be $T_e(A\,^2\Sigma^-) \approx 10\,300$ cm^{-1} above the $X\,^2\Pi_{1/2}$ state. The *ab initio* prediction,[8] which did not include treatment of the spin-orbit interaction, predicts a T_e (=3449 cm^{-1}) which is significantly less than the estimated $T_e(A\,^2\Sigma^-) \approx 10\,300$ cm^{-1} obtained here. The effects of the ignored Pt spin-orbit interaction for the states investigated in Ref. 8, however, are large. Consider, for example, the changing T_e value of the $a\,^4\Sigma^-$ state, for which spin-orbit interaction was treated in the calculations: in the absence of spin-order interaction, $T_e(a\,^4\Sigma^-)$ is calculated to be 975 cm^{-1}, yet the relativistic CI calculation of the lowest excited $\Omega = \frac{1}{2}$ state, which is 88% $^4\Sigma^-$, predicts $T_e(a\,^4\Sigma^-) =$ 5072 cm^{-1}. The $a\,^4\Sigma^-$ and $A\,^2\Sigma^-$ states arise from the same dominant $\cdots 3\sigma^1 2\pi^2$ configuration and it can be inferred that the true T_e value of the $A\,^2\Sigma^-$ state will be significantly higher than the T_e (=3449 cm^{-1}) calculated in the absence of spin-orbit interaction. The 6s orbital is strongly stabilized via relativistic effects[22] and the separation between the $A\,^2\Sigma^-$ and the $X\,^2\Pi$ states is expected to be underestimated when relativistic effects are not included because the $3\sigma \rightarrow 2\pi$ excitation is essentially a promotion of a 6s electron.

The ^{195}Pt (I = 1/2) hyperfine parameters provide the most detailed experimentally derived information about the nature of the $X\,^2\Pi_{1/2}$ and $A^2\Sigma^-$ states. Unfortunately, these parameters are rarely predicted in *ab initio* studies because

they depend upon very accurate electronic wavefunctions in the region of the nuclei. The common practice is to use an "atoms-in-molecules" approach that uses experimentally or theoretically derived atomic hyperfine information and a proposed atomic orbital composition of the relevant molecular orbitals. This approach was used successfully to provide a qualitative interpretation of the hyperfine structure in the $X\,^2\Pi_{1/2}$ state of platinum nitride, PtN, by Jung *et al.*,[7] and more recently for the hyperfine interaction of the $X\,^2\Pi_{3/2}$ state of platinum monofluoride, PtF.[23]

In the case of the $A^2\Sigma^-$ state, which has no electronic orbital angular momentum, only the Fermi contact and dipolar contributions of Eq. (6) are relevant. The Fermi contact, b_F, and dipolar, c, parameters are defined as[17,24]

$$b_F/\mathrm{Hz} = \left(\frac{\mu_0}{4\pi h}\right)\left(\frac{8\pi}{3}\right) g_e g_N \mu_B \mu_N \frac{1}{\Sigma} \times \langle \Lambda, \Sigma = S| \sum_i \hat{s}_{zi}\delta_i(r)|\Lambda, \Sigma = S\rangle, \quad (7)$$

$$c/\mathrm{Hz} = \left(\frac{\mu_0}{4\pi h}\right)\frac{3}{2} g_e g_N \mu_B \mu_N \frac{1}{\Sigma} \times \langle \Lambda, \Sigma = S| \sum_i \hat{s}_{zi}\frac{(3\cos^2\theta_i - 1)}{r_i^3}|\Lambda, \Sigma = S\rangle. \quad (8)$$

In Eqs. (7) and (8), $\hat{s}_{zi}$ is the spin angular momentum operator for the ith electron, δ_i(r) is a Dirac delta function, and r and θ are polar coordinates. The $\frac{1}{\Sigma}$ factors in Eqs. (7) and (8) account for the fact that the effective Hamiltonian used to fit the data was written in terms of total spin and orbital angular momenta, whereas the definitions of b_F and c are from integrals of one-electron operators. The symmetry adapted wavefunction for a $^2\Sigma^-(\pi^2\sigma)$ state is the linear combination of Slater determinants[25]

$$\psi(^2\Sigma^-[\pi^2\sigma]) = \frac{1}{\sqrt{6}}(2\left|\pi^+\pi^-\bar{\sigma}\right| - \left|\pi^+\bar{\pi}^-\sigma\right| - \left|\bar{\pi}^+\pi^-\sigma\right|), \quad (9)$$

where, for example, $\bar{\pi}^+$ is the π, $\lambda = +1$, $m_s = -1$ spin-orbital. The expectation value that appears in b_F is readily obtained using the rules for evaluation of Slater determinants,[26] resulting in

$$b_F = -\frac{1}{3}\left(95.4129\,\mathrm{MHz/a.u.}^3\right) g_I \frac{8\pi}{3}\langle 3\sigma|\,\delta(0)\,|3\sigma\rangle = -\frac{1}{3}\left(95.4129\,\mathrm{MHz/a.u.}^3\right) g_I \frac{8\pi}{3}|\Psi(0)|^2, \quad (10)$$

where $|\Psi(0)|^2$ is the spin-density at the Pt-nucleus, and the conversion factor, 95.4129 MHz/a.u.$^{-3}$, assumes that the unit for the expectation value is a.u.$^{-3}$ Similarly, the dipolar parameter is given as

$$c = +\frac{4}{3}\times(95.4129\,\mathrm{MHz/a.u.}^3)\times g_I \times \langle 2\pi|\frac{3\cos^2\theta - 1}{r^3}|2\pi\rangle. \quad (11)$$

Estimates for the expectation values that appear in the expressions for b_F and c can be derived from atomic magnetic hyperfine information if it is assumed that the 2π and 3σ orbital are pure Pt-centered $5d_{\pm1}$ and $6s$ orbitals, respectively. Within a single $nl^n n's$ configuration (e.g., $5d^9 6s^1$ of Pt), the atomic magnetic hyperfine operator is[27,28]

$$\hat{H}_{mhf} = \sum_{i=1}^{N}\left[\hat{l}_i a_{nl}^{01} - (10)^{1/2}(\hat{s},\hat{C}^2)_i^1 a_{nl}^{12} + \hat{s}_i a_{nl}^{10}\right]\cdot\hat{I} + a_{n's'}^{10}\hat{s}_{n'}\cdot\hat{I}, \quad (12)$$

where $\hat{l}_i$, $(\hat{s},\hat{C}^2)_i^1$, and $\hat{s}_i$ are the orbital, spin dipolar, and spin operators for the electrons with orbital angular momenta, and $\hat{s}_{n'}$ is the electron spin operator for the unpaired s-electron. The four effective atomic hyperfine parameters, a_{nl}^{01}, a_{nl}^{12}, a_{nl}^{10}, and $a_{n's}^{10}$ are defined as

$$a_{nl}^{ij} = 95.4128(\mathrm{MHz/a.u.}^{-3})g_I\langle r^{-3}\rangle_{nl}^{ij} \quad (13)$$

and

$$a_{n's}^{10} = 95.4128(\mathrm{MHz/a.u.}^{-3})g_I\langle r^{-3}\rangle_{n's}^{10}, \quad (14)$$

where the conversion factor assumes that the units for $\langle r^{-3}\rangle_{nl}^{ij}$ and $\langle r^{-3}\rangle_{n's}^{10}$ are a.u.$^{-3}$. In the nonrelativistic limit, $\langle r^{-3}\rangle_{n's}^{10} = \frac{8\pi}{3}|\Psi_{n's}(0)|^2$. Under the assumption that the 2π and 3σ orbitals are pure Pt-centered $5d_{\pm1}$ and $6s$ orbitals, respectively, then

$$b_F = -\frac{1}{3}\left(95.4129\,\mathrm{MHz/a.u.}^3\right) g_I\langle r^{-3}\rangle_{6s}^{10} \quad (15)$$

and

$$c = +\frac{4}{3}\times\left(95.4129\,\mathrm{MHz/a.u.}^3\right) g_I\frac{2}{7}\langle r^{-3}\rangle_{5d}^{12}. \quad (16)$$

The 2/7 factor in Eq. (16) is the expectation value $\langle d_{\pm1}|(3\cos^2\chi - 1)|d_{\pm1}\rangle$.

Büttgenbach *et al.*[29] simultaneously modelled 11 atomic hyperfine A factors for levels arising from the $5d^9 6s^1$ and $5d^8 6s^2$ configurations of atomic Pt, three of which were precisely measured by atomic beam magnetic resonance (ABMR) techniques and the remaining 8 less precisely by optical spectroscopy, to determine $\langle r^{-3}\rangle_{5d}^{01}$, $\langle r^{-3}\rangle_{5d}^{12}$, $\langle r^{-3}\rangle_{5d}^{10}$, and $\langle r^{-3}\rangle_{n's}^{10}$ of 11.01 a.u.$^{-3}$, 4.26 a.u.$^{-3}$, −2.29 a.u.$^{-3}$, and 256.7 a.u.$^{-3}$, respectively. It was assumed that $\langle r^{-3}\rangle_{nl}^{ij}$ for the $5d^8 6s^2$ and $5d^9 6s^1$ configurations were identical. Soon thereafter, Neu *et al.*[30] re-measured the optical spectrum and performed an analysis similar to that of Büttgenbach *et al.*[29] to determine values for $\langle r^{-3}\rangle_{5d}^{01}$, $\langle r^{-3}\rangle_{5d}^{12}$, $\langle r^{-3}\rangle_{5d}^{10}$, and $\langle r^{-3}\rangle_{n's}^{10}$ of 10.51 a.u.$^{-3}$, 12.78 a.u.$^{-3}$, 0.25 a.u.$^{-3}$, and 264 a.u.$^{-3}$, respectively. An *ab initio*[31] calculation employing an Optimized Hartree-Fock Slater (OHFS) method predicted $\langle r^{-3}\rangle_{5d}^{01}$, $\langle r^{-3}\rangle_{5d}^{12}$, $\langle r^{-3}\rangle_{5d}^{10}$, and $\langle r^{-3}\rangle_{n's}^{10}$ of 12.389 a.u.$^{-3}$, 15.633 a.u.$^{-3}$, −1.404 a.u.$^{-3}$, and 273.3 a.u.$^{-3}$, respectively. The atomic values of Refs. 29–31 for $\langle r^{-3}\rangle_{6s}^{10}$ substituted into Eq. (15) predict a b_F value of −9952 MHz, −10 224 MHz, and −10,568 MHz, respectively. Similarly, the atomic values of Refs. 29–31 for $\langle r^{-3}\rangle_{5d}^{12}$ substituted into Eq. (16) predict a c value of +189 MHz, +566 MHz, and +660 MHz, respectively. The atomic value for $\langle r^{-3}\rangle_{5d}^{12}$ from Ref. 29 appears to be inconsistent with the other two.

The simple atoms-in-molecule prediction of a larger negative ^{195}Pt $b_F \sim -10\,000$ MHz is consistent with the observation value of -8559 ± 45 MHz. The *ab initio* prediction[8] indicates that the $(\upsilon = 2)$ $A\,^2\Sigma^-$ state has a dominant (84%) $\cdots 3\sigma^1 2\pi^2$ electron configuration, but, as mentioned above, did not include treatment of spin-orbit interaction. If it assumed that the other configurations do not contribute to b_F, then the simple model prediction for b_F is ~ -8400 MHz $(= -10\,000$ MHz $\times\, 0.84)$, suggesting that the 3σ orbital is essentially 100% 6*s* character. It is noteworthy that the Mulliken population analysis[8] predicts a gross population for Pt(6*s*) of 0.862 for the $A\,^2\Sigma^-$ state.

The simple atoms-in-molecule model predicts a small, positive, *c* parameter (~600 MHz), whereas the experimentally determined value is a small, poorly determined, negative value of -0.028 ± 0.010 cm^{-1} $= -840 \pm 300$ MHz. It was noted in the *ab initio* predictions[7,8] that the 2π orbital is strongly polarized towards the N-center (i.e., has a major $2p$(N) contribution), which is not accounted for in the simple prediction performed here. Furthermore, an admixture of Pt($6p_{\pm 1}$) to the 2π orbital, which has been assumed to be a pure Pt-centered $5d_{\pm 1}$ in the present analysis, could produce a negative *c* parameter because $\langle p_{\pm 1}|(3\cos^2\chi - 1)|p_{\pm 1}\rangle = -2/5$.

The ^{14}N hyperfine parameters are very well determined for both $X\,^2\Pi_{1/2}$ and $A\,^2\Sigma^-$states (see Table II). In the $X\,^2\Pi_{1/2}$ state, $h_{1/2}(^{14}\text{N})$ and d(N) are determined to be 64 $\pm$ 2 MHz and 62 $\pm$ 3 MHz, respectively. The proposed dominant $\cdots 3\sigma^2 2\pi^1$ electronic configuration suggests that $b_F = 0$ and therefore $h_{1/2} = a - c/3$. Assuming that the sole unpaired electron occupies the N–centered $2p_{\pm 1}$ orbital, the *a* parameter is given by

$$a(X^2\Pi_{1/2})(\text{Hz}) = \left(\frac{\mu_0}{4\pi h}\right) 2 g_N \mu_B \mu_N \left\langle 2p_{\pm 1}\right| r^{-3} \left|2p_{\pm 1}\right\rangle. \tag{17}$$

An expression analogous to Eq. (8) was used to predict the *c* parameter. Assuming that the 2π orbital is a pure N-centered $2p_{\pm 1}$ and using the *ab initio* predicted value of 3.0997 a.u.$^{-3}$ for $\langle 2p|r^{-3}|2p\rangle$ given in Ref. 32, then $a(X^2\Pi_{1/2})$ and $c(X^2\Pi_{1/2})$ parameters are calculated to be 118 MHz and -81 MHz, respectively. Combining *c* and *a*, the simple molecular orbital model predicts that $h_{1/2}(^{14}\text{N}) = 144$ MHz. The predicted Mulliken population analysis[8] indicates that the 2π orbital is only 36% of the N-centered $2p_{\pm 1}$ orbital in the bonding. Thus, the atoms-in-molecule prediction, coupled with the *ab initio* Mulliken population, gives $h_{1/2}$(N) of 52 MHz, which is in good agreement with the observed value of 63 MHz. Basically, the simple model predicts a small positive value for $h_{1/2}(^{14}\text{N})$ for the $X\,^2\Pi_{1/2}$ state, which is consistent with the observation.

The ^{14}N hyperfine parameters b_F and *c* for the $A\,^2\Sigma^-$ state are determined to be 20 $\pm$ 2 MHz and -58 ± 6 MHz, respectively. The proposed dominant $\cdots 3\sigma^1 2\pi^2$ configuration for the $A\,^2\Sigma^-$ state would, according to Eq. (10), predict a small negative value for b_F if the 3σ had a significant contribution from either the N-centered $2s$ or $3s$ orbitals. The observed small positive value can be rationalized as spin–polarization of the Pt-N bond by the Pt-centered unpaired electrons. Using Eq. (11), the *ab initio* predicted value of 3.0997 a.u.$^{-3}$ for $\langle 2p|r^{-3}|2p\rangle$ from Ref. 32, and $\langle p_{\pm 1}|(3\cos^2\chi - 1)|p_{\pm 1}\rangle = -2/5$, *c* is predicted to be -64 MHz. A comparison with the observed value of -58 ± 6 MHz suggests that the 2π orbital is strongly polarized towards the N–center (i.e., has a major $2p$(N) contribution) as noted in the *ab initio* predictions.[7,8] Basically, the simple model predicts a small negative $c(^{14}\text{N})$ for the $A\,^2\Sigma^-$ state, which is not consistent with the observation.

CONCLUSIONS

The electronic structure properties of PtN have been well characterized by both intracavity laser spectroscopy and high-resolution molecular beam laser induced fluorescence. For the ground state, the determined $X\,^2\Pi_{1/2}$ parameters are in good agreement with the previous measurement.[7] The ^{14}N hyperfine parameters were determined experimentally for the first time. A simple molecular-orbital based model predicts a small positive value for effective magnetic hyperfine parameter $h_{1/2}(^{14}\text{N})$ for the $X\,^2\Pi_{1/2}$ state, which is consistent with observation.

The excited state associated with the near infrared electronic transition has been assigned as the $\upsilon = 2$ level of the $A\,^2\Sigma^-$ electronic state. The origin of this state is not well predicted by the previous electronic structure calculation.[8] The ^{195}Pt and ^{14}N magnetic hyperfine interactions in the $\upsilon = 2$ $A\,^2\Sigma^-$ state have been determined and used in a simple "atoms-in-molecule" model to garner insight into the nature of the $A\,^2\Sigma^-$ electronic state. The hyperfine parameters are consistent with a dominant $\cdots 3\sigma^1 1\pi^4 2\pi^2 1\delta^4$ configuration for the $A\,^2\Sigma^-$ electronic state. A comparison of the observed $b_F(^{195}\text{Pt})$ and $c(^{14}\text{N})$ magnetic hyperfine parameters with those predicted by the simple model suggest that the 3σ orbital has 82% Pt-centered 6*s* character and the 2π orbital is nearly pure N-centered, which is in qualitative agreement with the molecular orbital correlation diagram and the *ab initio* predictions.[7,8]

Magnetic hyperfine interactions are the most sensitive probe of the electronic wavefunction, particularly in the region of the nuclei with non-zero spin. Hence, a comparison of experimentally derived values with those predicted from *ab initio* calculations is an ideal method for assessing various computational methodologies. Predicting the values for the magnetic hyperfine parameters determined in the present study for the simple, two nuclear spin, diatomic molecule PtN should be the goal of future electronic structure studies.

ACKNOWLEDGMENTS

Funding for this work was provided by the Division of Chemistry at the National Science Foundation, Grant Nos. CHE-1112354 (JJOB) and CHE-1112301 (LCOB). T.C.S. contribution was supported by a grant from Fundamental Interactions Branch, Division of Chemical Sciences, Office of Basic Energy Sciences, Department of Energy (Grant No. DE-FG02-01ER15153-A003). The authors thank Dr. Colin Western (School of Chemistry, University of Bristol, UK, BS8 1TS) for his assistance with the PGOPHER program.

[1]G. L. Miessler and D. A. Tarr, *Inorganic Chemistry* (Prentice-Hall, New Jersey, 1991).
[2]D. B. Dell'Amico, L. Labella, F. Marchetti, and S. Samaritani, Coord. Chem. Rev. **254**, 635–645 (2010).
[3]D. J. Harding and A. Fielicke, Chem. Eur. J. **20**, 3258–3267 (2014).
[4]H. Yamamoto, K. Miyajima, T. Yasuike, and F. Mafuné, J. Phys. Chem. A **117**, 12175–12183 (2013).
[5]M. Schlangen and H. Schwartz, Catal. Lett. **142**, 1265–1278 (2012).
[6]E. J. Friedman-Hill and R. W. Field, J. Chem. Phys. **100**, 6141–6152 (1994).
[7]K. Y. Jung, T. C. Steimle, D. Dai, and K. Balasubramanian, J. Chem. Phys. **102**, 643–652 (1995).
[8]D. Dai and K. Balasubramanian, J. Mol. Spectrosc. **172**, 421–429 (1995).
[9]K. G. Handler, R. A. Harris, L. C. O'Brien, and J. J. O'Brien, J. Mol. Spectrosc. **265**, 39–46 (2011).
[10]L. C. O'Brien, H. Cao, and J. J. O'Brien, J. Mol. Spectrosc. **199**, 100–108 (2000).
[11]S. Gerstenkorn, J. Vergès, and J. Chevillard, *Atlas du Spectre d'Absorption de la Molécule d'Iode 11 000–14 000 cm^{-1}* (Laboratoire Aimé Cotton, CNRS II, Orsay, 1982).
[12]L. C. O'Brien, H. Cao, and J. J. O'Brien, J. Mol. Spectrosc. **207**, 99–103 (2001).
[13]See supplementary materials at http://dx.doi.org/10.1063/1.4893703 for tables of assignments, line positions and residuals for ^{194}PtN, ^{195}PtN, and ^{196}PtN.
[14]G. Herzberg, *Molecular Spectra and Molecular Structure, I. Spectra of Diatomic Molecules*, 2nd ed. (Van Nostrand, Princeton, New Jersey, 1975).
[15]C. M. Western, PGOPHER, a program for simulating rotational structure, University of Bristol, 2014, see http://pgopher.chm.bris.ac.uk.
[16]E. Hirota, *High-Resolution Spectroscopy of Transient Molecules* (Springer-Verlag, Berlin, Heidelberg, New York, Tokyo, 1985).
[17]R. A. Frosch and H. M. Foley, Phys. Rev. **88**, 1337–49 (1952).
[18]C. H. Townes and A. L. Schawlow, *Microwave Spectroscopy* (Dover Publications, New York, 1975).
[19]M. Hall and R. Fenske, Inorg. Chem. **11**, 768–775 (1972).
[20]T. C. Steimle, K. Y. Jung, and B. Li, J. Chem. Phys. **103**, 1767–1772 (1995).
[21]B. Hong, L. Cheng, M. Y. Wang, and Z. J. Wu, Mol. Phys. **108**, 25–33 (2010).
[22]P. Pyykkö, Annu. Rev. Phys. Chem. **63**, 45–64 (2012).
[23]C. Qin, R. Zhang, F. Wang, and T. C. Steimle, J. Chem. Phys. **137**, 054309 (2012).
[24]J. M. Brown and A. Carrington, *Rotational Spectroscopy of Diatomic Molecules* (Cambridge University Press, Cambridge, 2003).
[25]J. Raftery, P. R. Scott, and W. G. Richards, J. Phys. B **5**, 1293–1301 (1972).
[26]M. Weissbluth, *Atoms and Molecules* (Academic Press, New York, 1978).
[27]W. J. Childs, Phys. Rev. **156**, 71–81 (1967).
[28]S. Büttgenbach, *Hyperfine Structure in 4d and 5d-Shell Atoms* (Springer Tracts in Modern Physics, Springer-Verlag, Berlin, 1982).
[29]S. Büttgenbach, N. Glaeser, B. Roski, and F. Täeber, Z. Phys. A **317**, 237–240 (1984).
[30]W. Neu, G. Passler, G. Sawatzky, R. Winkler, and H.-J. Kluge, Z. Phys. D **7**, 193–201 (1987).
[31]G. Olsson and A. Rosén, Phys. Scr. **26**, 168–182 (1982).
[32]J. A. J. Fitzpatrick, F. R. Manby, and C. M. Western, J. Chem. Phys. **122**, 084312 (2005).